

Estimating the cost of high temperature liquid metal based concentrated solar power

Cite as: J. Renewable Sustainable Energy **10**, 023705 (2018); <https://doi.org/10.1063/1.5014054>
Submitted: 14 November 2017 . Accepted: 06 March 2018 . Published Online: 26 March 2018

Gregory Wilk, Alfred DeAngelis, and Asegun Henry



View Online



Export Citation



CrossMark

ARTICLES YOU MAY BE INTERESTED IN

[Pumped thermal grid storage with heat exchange](#)

Journal of Renewable and Sustainable Energy **9**, 044103 (2017); <https://doi.org/10.1063/1.4994054>

[Solar energy harvesting wireless sensor network nodes: A survey](#)

Journal of Renewable and Sustainable Energy **10**, 023704 (2018); <https://doi.org/10.1063/1.5006619>

[Review and future perspective of central receiver design and performance](#)

AIP Conference Proceedings **1850**, 030052 (2017); <https://doi.org/10.1063/1.4984395>

Scilight Highlights of the best new research
in the physical sciences

[LEARN MORE!](#)



Estimating the cost of high temperature liquid metal based concentrated solar power

Gregory Wilk,¹ Alfred DeAngelis,¹ and Asegun Henry^{1,2,3}

¹George W. Woodruff School of Mechanical Engineering, Georgia Institute of Technology, Atlanta, Georgia 30318, USA

²School of Materials Science and Engineering, Georgia Institute of Technology, Atlanta, Georgia 30318, USA

³Heat Lab, Georgia Institute of Technology, Atlanta, Georgia 30318, USA

(Received 14 November 2017; accepted 6 March 2018; published online 26 March 2018)

The current levelized cost of electricity from concentrated solar power is too high to directly compete with natural gas under current carbon emissions policies. An approximate 50% cost reduction is needed relative to current power tower technology based on molten nitrate salts, and one pathway to a major cost reduction is to operate the system at higher temperatures, enabling a more efficient heat engine. Here, we consider a future system that can operate at gas turbine inlet temperatures of $\sim 1300\text{--}1500\text{ }^{\circ}\text{C}$ by using liquid metals as heat transfer and storage fluids with a ceramic based piping infrastructure. In general, ceramics are more expensive than the current stainless steels, but they are less expensive than the nickel alloys that are proposed to be used in higher temperature chloride molten salt plants. Considering various tradeoffs, it was not clear *a priori* whether or not the potential gains in heat engine efficiency would be negated by increased material costs or how much net reduction in levelized cost might be possible. This study answers this question by first detailing a base case molten nitrate salt power tower plant with published cost data. Then, a future liquid metal version of a power tower is modeled using similar specifications as the liquid salt plant to determine if there are any obvious costs that might negate the efficiency gains associated with operating well above $1000\text{ }^{\circ}\text{C}$. The results of the analysis showed that although the receiver and several other sub-systems become more expensive, there is a net cost reduction in the range of 20%–30%, depending upon the heat engine efficiency. Published by AIP Publishing. <https://doi.org/10.1063/1.5014054>

NOMENCLATURE

CSP	Concentrated solar power
HTF	Heat transfer fluid
HX	Heat exchanger
LCOE	Levelized cost of electricity
LDHX	Liquid droplet heat exchanger
LM	Liquid metal
LM-CSP	Liquid metal concentrated solar power
LMTD	Log mean temperature difference
LS	Liquid salt
LS-CSP	Liquid salt concentrated solar power
NREL	National Renewable Energy Laboratory
SAM	System advisor model
SC	Secondary concentrator
STHX	Shell and tube heat exchanger
TES	Thermal energy storage
TIT	Turbine inlet temperature
WAM	Westmoreland Advanced Materials

I. INTRODUCTION

In examining the options for renewable energy at the grid level, there are two commercialized approaches for directly utilizing solar energy, namely, photovoltaics (PV) and concentrated solar power (CSP). Currently, PV is less expensive than CSP on a cost per unit power output basis, with a predicted 2020 levelized cost of electricity (LCOE) that ranges from 3 to 12 ¢/kWh_e,¹ compared to that of CSP systems which ranges from 7 to 20 ¢/kWh_e.² However, the major distinction between the two technologies is storage. Storing electricity from PV with electrochemical batteries would increase the cost beyond that of CSP, which can naturally integrate thermal energy storage (TES).^{1,3} Furthermore, for batteries, the amount of energy stored is somewhat coupled to the rate of discharge and there is typically a tradeoff between the lifetime and the discharge rate for batteries, which plays a major role in its high cost.^{4,5} For TES, on the other hand, these issues are non-existent and the energy stored is almost completely decoupled from the rate of discharge with very long lifetimes.^{6,7}

A CSP tower plant with TES is composed of four primary subsystems: a heliostat field, a receiver, TES, and a power block (Fig. 1).⁶ The heliostat field consists of many mirrors, typically 1000–100 000 that cover an area on the order of 1–3 km², which concentrates sunlight onto a central tower.^{8,9} The concentrated sunlight incident on the receiver is then absorbed, and the energy is transferred as heat to a heat transfer fluid (HTF), which can be liquid salt (LS) for TES or can be used to directly heat water/steam.^{9–11} When electricity is needed in a system with TES, the storage fluid is pumped from the hot tank through a heat exchanger (HX) to a cold storage tank. The HX transfers heat from the storage medium/fluid to a power cycle working fluid, which is currently steam for a Rankine cycle in LS-CSP plants (Fig. 1).¹²

Commercial LS-CSP power tower plants have been built, including a 100 MW_e Solar Reserve plant in Tonopah, NV, with 10 h of energy storage and the 20 MW_e Gemasolar plant in Spain with 15 h of storage.⁹ Both plants provide dispatchable electricity to the grid with an estimated LCOE of 13–20 ¢/kWh_e. Newer CSP plants have been proposed with LCOE ranging from 7 to 9 ¢/kWh_e in countries with favorable financing and ideal solar resources.¹³ In many areas with lower solar insolation, current costs are too high to compete with combined cycle natural gas plants which range from 6 to 11 ¢/kWh_e.^{6,14,15} One pathway to reduce CSP costs is to increase the turbine inlet temperature (TIT) of the CSP plant and increase the power cycle efficiency. Current LS-CSP plants operate with a TIT of ~565 °C and use a Rankine power cycle with conversion efficiencies of ~36%–40%.^{6,9,14} More efficient alternative power cycles exist, including commercial combined cycle natural gas plants which operate >1200 °C and have conversion efficiencies of ~55%–60%, which is a 50% increase over Rankine power cycles and therefore has the potential to reduce the LCOE by up to ~33%.^{16,17} A further increase in LS-CSP plant operating temperature is currently limited by corrosion of the 316 SS infrastructure as well as chemical stability of the molten nitrate salts (NaNO₃-KNO₃ eutectic), which degrade above 600 °C.^{18–21}

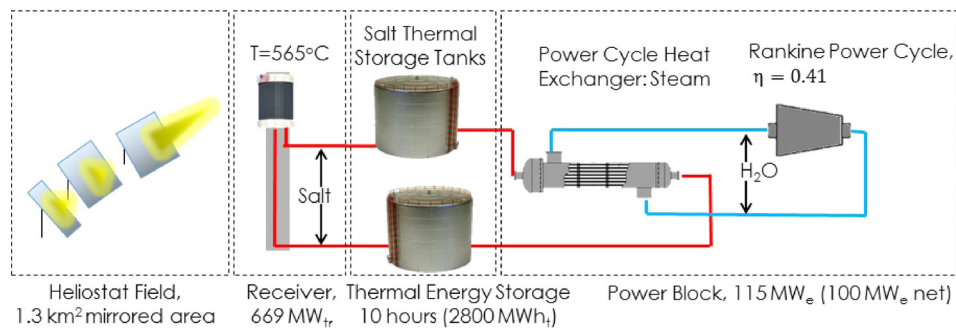


FIG. 1. Molten salt plant schematic illustrating the four primary subsystems used to convert sunlight to heat, which is then stored and later converted to electricity. The subscripts “tr,” “t,” and “e” denote the origin of heat energy as “thermal receiver,” “thermal TES,” and “electrical,” respectively.

II. THE CONCEPTUAL LIQUID METAL (LM) CSP PLANT CONFIGURATION AND LAYOUT

Alternative fluids to molten nitrate salts are under consideration to enable higher TITs, including molten glass,²² chloride and fluoride salts,^{23,24} solid particles,^{25,26} and liquid metals (LMs).^{27,28} Solid particles appear to be one of the most attractive options because they are inexpensive materials and have minimal corrosion.^{26,29} However, new falling particle receivers must be developed, which must overcome challenges in managing the heat transfer in a gravity driven particle flow, which has presented challenges in attaining high efficiencies >75% and reaching peak TITs with less than peak solar input.^{30,31} Also, how heat will be transferred from the particles to the power cycle is a potential challenge.³² In this respect, pumped liquids have an advantage since they do not need to rely on gravity and can be more easily controlled and ramped up or down with a minimal effect on the receiver performance, assuming that the required pumping power is small. LMs, such as tin (Sn) and aluminum silicon (Al-Si) alloys, are a viable option for high temperature (~1400 °C) CSP due to their chemical stability and low vapor pressure.^{28,33} LMs have an additional low pumping power advantage, due to their high thermal conductivity, which is more than an order of magnitude higher than non-electrically conductive fluids such as molten salts, water, and oil. Higher thermal conductivity significantly reduces the flow speeds required for effective convective heat transfer and therefore reduces the pump power requirement. This paper presents a conceptual design for a LM-CSP plant where Sn was chosen as the HTF due to its low melting temperature (232 °C) and chemical compatibility with high thermal conductivity refractory ceramics such as graphite and silicon carbide (SiC).^{34,35} Al-Si is envisioned as the TES medium, due to its much lower cost than Sn, as discussed earlier.

While LMs are a potential HTF for high temperature high efficiency CSP, in general, one cannot use metals, such as stainless steel for containment, since they would be quickly dissolved/corroded by LMs at 1400 °C.^{19,23,36,37} Another class of materials, namely, ceramics, however, can be thermodynamically stable with respect to the LMs of interest at high temperatures.³⁴ Thermodynamic stability implies that there is no chemical reaction or dissolution that will occur at any time scale, and one need not rely on a kinetically limited mechanism as is the case for 316 SS and molten salt. In this sense, thermodynamically stable material combinations are rarely found in industrial applications, let alone at high temperatures, but this is a principle benefit of utilizing ceramics for CSP. Our recent prototype demonstrations of high temperature liquid metal pumping pioneered by Amy *et al.*³⁸ also significantly reduced the technical uncertainty of LM-CSP. In this recent work, we demonstrated for the first time that liquid Sn could be pumped at temperatures ranging from 1200 to 1400 C, using all ceramic/graphite gears, dynamic seals, and joints. The brittle nature of the ceramics was overcome by carefully managing the stresses experienced by the components to remain far below their fracture thresholds. Ceramic components such as pipes were insulated and then strapped to aluminum supports that carried their weight and any other induced forces or mechanical moments generated by the infrastructure. This strategy of insulating ceramic components so that structural metal supports at room temperature can carry the mechanical loads can also be scaled to a full plant design to prevent brittle fracture. The problem, however, is that ceramics in general cost more than the current steels used in LS-CSP. Thus, the most critical question we seek to answer in this study is whether or not there is a net LCOE reduction, when one weighs the higher cost ceramic infrastructure against the gains in efficiency associated with operating at higher TITs. In the subsequent high level analysis, this question will be answered by conceptually designing a LM-CSP plant, estimating the cost of all components and labor, and comparing them against their LS-CSP equivalents.

It should be noted that an increased cost associated with the ceramic containment infrastructure is not the only potential cost increase. Another issue is the fact that the receiver must be redesigned as a cavity receiver with secondary concentrators (SCs) that deliver $\geq 5 \text{ MW/m}^2$ fluxes³⁹ to an optical cavity containing the receiver tubes. This must be done to limit the view factor from the hotter (>1400 °C) surfaces to the environment; otherwise, the improvements in power cycle efficiency could be easily negated by re-radiation heat losses back to the

surroundings.^{27,39} Furthermore, the LMs of interest interact with oxygen and water vapor,^{24,28} and so, the entire system should be maintained in a sealed containment structure to prevent the penetration of the reacting gases (O_2), thereby holding the system in a low oxygen partial pressure environment. It is critical to appreciate that this requirement would apply to both chloride salts and LMs and thus can be considered a likely requirement for higher temperature CSP using liquids in general. Finally, since Sn is too expensive as a TES fluid ($> \$2\text{--}8/\text{lb} \rightarrow 27\text{--}110 \text{ \$/kWh}_t$), even if used between 300 and 1400 °C, a separate TES fluid, namely, Al-Si, is needed, which therefore necessitates additional HXs. Such HXs increase the capital costs and parasitic pumping loads, but it was not initially clear if such components would negate all the benefits of higher efficiency via higher TIT. Thus, the remaining analysis was dedicated to answering these questions by conceptually designing/envisioning a LM-CSP plant and estimating its various cost tradeoffs, etc.

The overall LM-CSP system design analyzed herein is shown in Fig. 2, whereby during the day, a portion of the thermal energy gathered from the receiver is used to charge the TES, while the remainder is used to directly heat the power cycle working fluid to produce electricity. After the sun sets, the TES tanks are discharged to provide heat for the power cycle as illustrated in Fig. 3. The temperatures in the system were chosen so that each HX would have the same difference in inlet and outlet temperatures: a log mean temperature difference (LMTD) of 14.4 °C during both TES charging and discharging with the lowest system temperature, 250 °C set to exceed the melting temperature of Sn, i.e., 232 °C. Many parameters for the LM-CSP plant were taken from the 100 MW_e LS-CSP base plant modeled by National Renewable Energy Laboratory (NREL's) System Advisor Model (SAM).^{40,41} For example, the heliostat field used in this LM-CSP plant is taken to be 1.05 times as large as the heliostat field modeled in NREL's design, which consisted of 8981 heliostats, each with a mirror area of 144 m², covering a land area of 7.7 km² with a nearly symmetric field layout optimized for Tonopah, NV. Optimizing the heliostat field for the higher concentrations required for a 1440 °C receiver was outside the scope of this initial assessment, and therefore, a larger heliostat field coupled with windowed secondary concentrators (SCs), which were assumed to be 97% reflective⁴² and 98% transparent, gave the LM-CSP plant the same thermal input as the published model LS-CSP plant. Here, it should be noted that the heliostat field size was increased by the inverse of the SC efficiency, which yielded a 5.3% larger and more expensive heliostat field than the LS-CSP design. Nonetheless, this choice rendered the total power incident on the receiver tubes identical for the two cases being considered. This allowed for a more

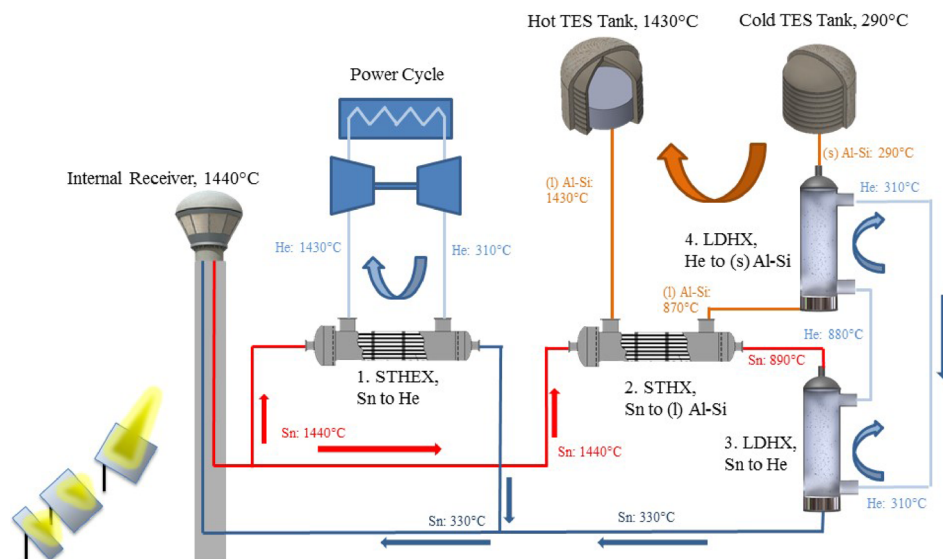


FIG. 2. LM-CSP plant schematic (flow indications for on-sun operation).

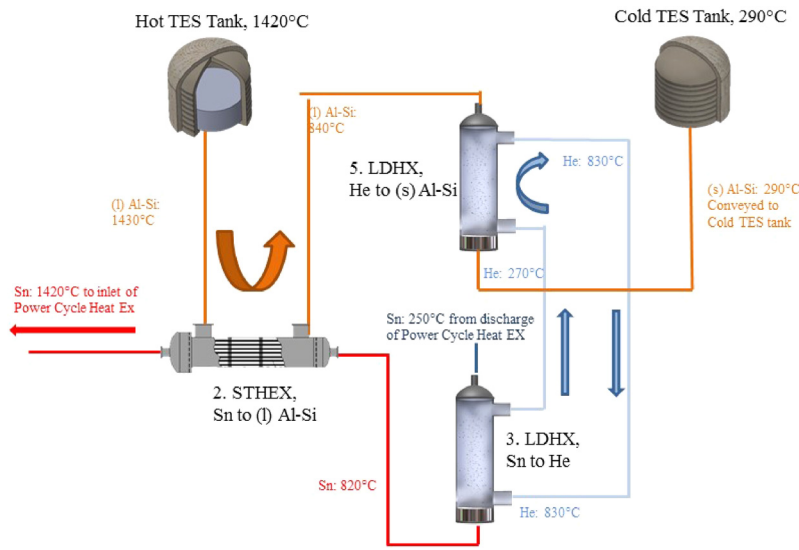


FIG. 3. TES discharge to the power cycle. HXs #2 and #3 were the same unit as those used for charging the TES system with reversed flows. LDHX #5 was a similar design to LDHX #4, but a separate unit because solid particles fall from the top during charging vs. liquid for discharging.

direct comparison between the thermal system for the two technologies since the primary differences considered herein are the cost of the thermal infrastructure (receiver, TES, and HXs) and the efficiency of the power cycle.

Since nearly the same heliostat field was used as the LS design, the concentrated area or spot size was the same between both designs, and so, the LM-CSP receiver was designed with the same outer dimensions as the LS-CSP receiver to collect all the concentrated sunlight and deliver the same thermal power input as the model LS-CSP plant (669 MW_t). The LM-CSP receiver was re-envisioned as an array of modular cavity receivers, each with its own secondary concentrator that boosts the concentration from the heliostat field ($\sim 1000\times$) by an additional $5\times$, to reach 5 MW/m² peak fluxes.³⁹ Higher concentrations are also possible, but previous work³⁹ showed that this concentration enabled 90% receiver efficiency, defined as the enthalpy change of the HTF divided by sunlight entering the cavity. Due to the receiver modularity, each SC cavity module could be angled with respect to the tower to include light from specific sections of the heliostat field.

Both graphite and SiC were considered as potential receiver tubing materials, due to their high thermal conductivities;^{43,44} however, graphite was chosen over SiC because it had higher thermal shock resistance than SiC, which was important due to temperature swings experienced by the receiver from day/night cycles. This was the reason, it was also preferable to use Sn in the receiver, instead of Al-Si everywhere, since the melting point for Sn (232 °C) was lower, similar to that of current molten salts, and therefore, the same heat tracing approaches could be used to keep it from freezing overnight. Furthermore, in previous work, graphite was one of the few refractory materials with sufficiently high thermal conductivity, necessary for efficient heat transfer between incident sunlight and the HTF.^{39,43} Graphite was also preferred because it was significantly less expensive to machine, which enabled less expensive custom headers, bends, joints, T-junctions, and interfaces throughout the receiver.

For the LM-CSP plant, an Al-Si alloy was used because it was less expensive than Sn (\$3.5/kWh_t vs. \$50/kWh_t) and it comprised most of the liquid volume/mass in the system. Here, Si was added to Al for the following two reasons: (1) it decreased the activity of Al and, at ~ 20 atom % Si, brought the alloy into thermodynamic equilibrium with SiC, preventing the formation of Al₃C₄; (2) it boosted the energy density from 1.67 MJ/kg for pure Al to 2 MJ/kg over the temperature range of 1440 °C–290 °C as is illustrated in Fig. 4. This was due to the high latent heat of Si, which was $\sim 3\times$ that of H₂O^{45,46} and other metals such as Fe.⁴⁷ In the

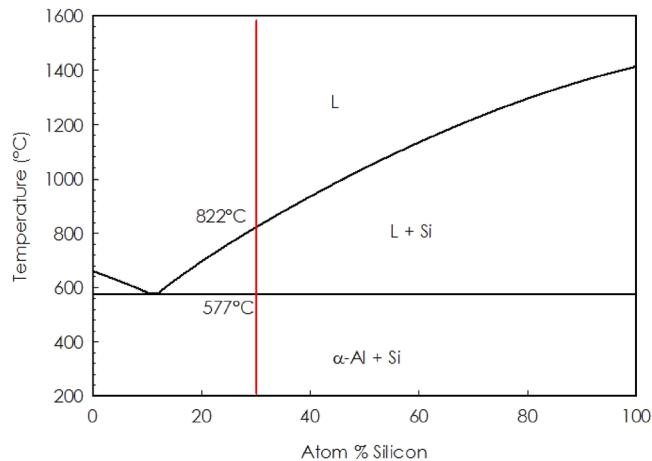


FIG. 4. Al-Si phase diagram.⁴⁵ The alloy chosen for TES is shown as the vertical red line, namely, 30 atom % Si. Latent heat was extracted in the temperature range of 577 °C–822 °C,⁴⁵ which matched well with the envisioned heat input temperatures for a SCO₂ cycle.

envisioned system, the Al-Si alloy was cycled from fully liquid at 1430 °C to fully solid at 290 °C with a two phase mixture Al-Si (s + l) from the liquidus temperature of 822 °C (Fig. 4) to the eutectic temperature of 577 °C (Ref. 45) for a 30 atom % Si alloy. The off-eutectic alloy is used here, instead of the eutectic composition consisting of 12.3 atom % Si, to make the alloy chemically compatible with SiC. Using an off-eutectic composition also served to increase the energy density, reducing the tank size, and also brought the range of solidification in alignment with the target input temperature range envisioned for supercritical CO₂ Brayton (SCO₂) cycles,^{48–50} which was an envisioned portion of the combined cycle that would be employed. Due to the phase change, a greater proportion of thermal energy was stored near the supercritical CO₂ TIT, 800 °C, thereby minimizing second law inefficiencies during heat transfer from sunlight to supercritical CO₂.

As illustrated in Fig. 2, to charge the TES, Sn heated Al-Si using 3 HXs: a shell and a tube heat exchanger (STHX) to heat liquid Al-Si (#2 in Fig. 2) to the peak temperature and two liquid droplet heat exchangers (LDHX)^{51–53} heated Al-Si (s) above its liquidus temperature (#4 in Fig. 2), using He (g) (#3 in Fig. 2) as an indirect/intermediate HTF that could be brought into direct contact with both LMs without any chemical interaction.

The STHX consisted of SiC tubes inside a SiC shell since SiC was simultaneously chemically inert with respect to Sn and Al-Si and has high thermal conductivity.⁵⁴ Such HXs are commercially manufactured by Saint Gobain, and the costs and tube dimensions associated with their products were used in the estimates described herein, based on budgetary quotes provided. During discharge, the LDHX consisted of an upward flowing He gas and a downward falling spray of liquid droplets, created by an array of nozzles like a shower head. The droplets fall by gravity, and for Al-Si, they solidified into solid particles during their descent, while they discharge their latent and sensible heat to He(g). Such HXs have been studied and tested previously^{51,52} for space power applications; however, significantly more research is required to prove that a LDHX can work as conceptualized. In this way, as illustrated in Fig. 2, two tandem direct contact HXs (LDHXs) enabled He gas to serve as an intermediate HTF between the two metals, whereby He (g) was chosen because it was the highest thermal conductivity noble gas at atmospheric pressure. Here, it should be emphasized that the system described in Fig. 2 operates with all LM at ambient pressure and the only pressurized portion of the system was the noble gas, i.e., the He/Ar mixture that moved through the power cycle was heated in the STHX by Sn.

Differential solidification is a potential problem with an off-eutectic Al-Si alloy, whereby regions with different compositions develop during solidification. Wang *et al.* studied molten Fe-Cu-Sn droplets falling through an inert gas and determined that phase separation was a

function of droplet size and cooling rate.⁵⁵ For the LM-CSP system described here, differential solidification could result in higher Si concentrations near the outer surfaces, which would raise the temperature required for re-melting the alloy and may alter the HX parameters somewhat. Future experiments are necessary to determine the exact LDHX parameters to ensure full melting over one charge/discharge cycle, and for simplicity, it was assumed that the envisioned configuration did not suffer from this problem.

In Fig. 2, Sn entered the first LDHX at 890 °C and fell through a column of He gas, heating it from 310 °C to 880 °C. The heated He then flowed upward through a second LDHX which heated Al-Si (s) from 290 °C, past its melting point starting at 577 °C, until it was fully liquid at 870 °C. The column walls of the LDHX were made of calcium aluminate castable cement (e.g., WAM AL-II), commercially available from Westmoreland Advanced Ceramics. This castable cement was chemically inert with respect to Al-Si and was also used as the solid containment material for the TES tanks.⁵⁶ The TES system was discharged to ultimately heat He/Ar for the power cycle by reversing the flows through the HXs as illustrated in Fig. 3. The LDHX between Al-Si and He had solid particles falling from the top during TES charging and liquid particles during TES discharge. While the top nozzle could be designed to handle both Al-Si phases, here they were modeled as two separate units: HX #4 and #5.

The power cycle subsystem consisted of a STHX (HX #1) made entirely of SiC and transferred heat between the Sn from the receiver or heated by the TES and the power cycle working fluid. The power cycle working fluid was envisioned to be a He/Ar mixture that was used to drive a closed cycle Brayton cycle, in tandem with a SCO₂ cycle, and/or possibly a steam Rankine bottoming cycle to achieve maximum efficiency.¹⁷ A detailed power cycle design was not pursued herein but was expected to achieve an efficiency in the range of 45%–65% depending upon the TIT and turbomachinery details. Therefore, the final LM-CSP LCOE is presented over a range of cycle efficiencies from the current LS-CSP baseline of 40% to an upper bound of 65%, which was an approximate thermodynamic limit.⁵⁷

The entire concept discussed herein has not been tested or proven in its entirety together, but many of the component level tests and proof of principle demonstrations have been done. For example, some of the critical components to the LM-CSP concept were the pumps, valves, piping, and joints, which presumably would need to be made entirely from ceramics at various locations throughout the circulation loop. Towards this end, initial demonstrations at a steady state temperature of 1200 °C and peak temperatures as high as 1400 °C have been accomplished without failure.³⁸ Further testing and improvement are needed to reach the long >10 000 h lifetimes needed for the LM-CSP concept, but the pathways to achieving this have been outlined.³⁸ Furthermore, extensive material compatibility testing has been done to verify that every material in contact, as described in the preceding, is chemically and thermodynamically stable (i.e., no corrosion), which will enable the materials to long live without failure.³⁴ Thus, although the many components have not been demonstrated together, there is strong evidence that with additional engineering, the aforementioned system could be realized since liquid metal challenges of material compatibility and 1400 °C pumping have been addressed.

III. COST ESTIMATION APPROACH

The U.S. National Renewable Energy Laboratory (NREL) created a detailed cost model template in the System Advisor Model (SAM),⁴⁰ and published details on a LS-CSP plant with 100 MW_e output and 10 h of thermal energy storage, which was in many ways similar in design and performance to the Tonopah plant built by Solar Reserve.⁴¹ Figure 5 shows a schematic created to show the technical parameters of the plant published by NREL, and the specifications are given in Table I.

NREL estimated 10 ¢/kWh_e for the LS-CSP LCOE;¹ however, individual component costs were not listed for the tower, receiver, TES tanks, salt media, and HX; therefore, Sandia's Power Tower Roadmap⁶ was used to provide these individual CSP components' cost, and their estimates are given in Table II. Sandia's component cost estimates were published in 2012, but NREL's 2016 update showed no change in the receiver, TES, and power cycle subsystem costs,

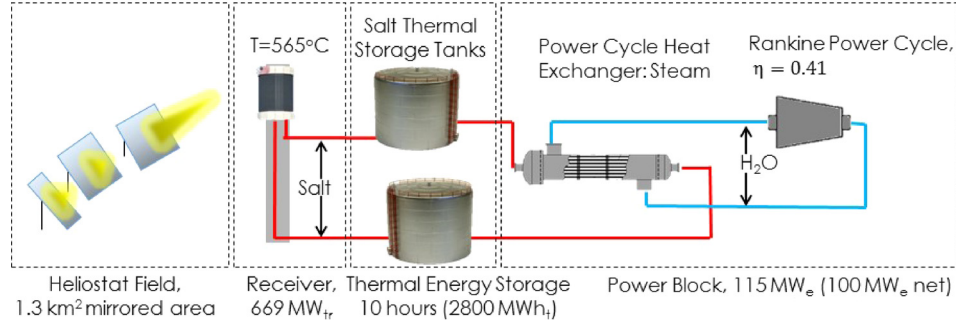


FIG. 5. Base model molten salt plant schematic illustrating the four primary subsystems used to convert sunlight to heat, which is then stored and later converted to electricity. The subscripts “tr,” “t,” and “e” denote the origin of heat energy as “thermal receiver,” “thermal TES,” and “electrical,” respectively.

TABLE I. Base model molten salt plant parameters.

Parameter	Performance
Heliostat field	1.3 km ² mirrored area
Receiver	669 MW _{tr} peak output
Solar multiple	2.4
TES capacity	10 h (2800 MWh _t)
Power cycle efficiency	41%
Power cycle gross output	115 MW _e
Plant parasitic loss	15 MW _e
Plant net electric output	100 MW _e

TABLE II. Major component costs in 2016 USD. The normalized cost units differ for different subsystems. The heliostat field cost was normalized to the mirror surface area (\$/m²). The receiver subsystem component costs were normalized to the receiver peak thermal power output (\$/kW_{tr}). The TES subsystem components were normalized to the energy storage capacity (\$/kWh_t). The power cycle components were normalized to the power cycle gross electric output, 115 MW (\$/kW_e). The second column normalizes all costs with respect to the modeled plant net electricity output of 100 MW_e (\$/kW_e).

	Normalized cost	Electric output normalized cost (\$/kW _e)	Cost fraction (%)
Heliostats	\$100/m ² (Ref. 1)	1300	34.6
Tower	\$25/kW _{tr} (Ref. 6)	168	4.5
Receiver	\$58/kW _{tr} (Ref. 6)	388	10.4
TES tanks	\$6/kWh _t (Ref. 6)	169	4.5
Salt media	\$12/kWh _t (Ref. 6)	336	9.0
Power cycle HX	\$214/kW _e (Ref. 6)	246	6.5
Power cycle	\$1000/kW _e (Ref. 6)	1150	30.6

and so, the LS-CSP component costs used for comparison in this paper were recently reported (2016). Heliostat field costs have reduced substantially since Sandia’s publication, and therefore, NREL’s more recent 2016 heliostat field estimate was used.

The liquid metal plant components described in Sec. II were modeled, and the costs were compared with their liquid salt versions detailed in Table II. The LM-CSP plant receiver thermal input and energy storage were identical to a LS-CSP design published by NREL.⁴⁰ This

enabled direct comparisons between published LS-CSP costs as well as final estimation of the change in LCOE of the two technologies. LM-CSP subsystem costs were modeled in two sections: Designed Subsystems and Non-Designed Subsystems. These sections describe the LM-CSP subsystems in detail and are included in the [supplementary material](#) section. Designed subsystems were systems that experienced significant redesign in the LM-CSP plant model as compared to the LS-CSP base case and include the tower, receiver, TES medium, TES tanks, five HXs, and nitrogen containment. LM component geometries were conservatively designed assuming steady state heat transfer and fluid flow. It is important to emphasize here that the term “design” implies a very high-level consideration of dimensions and characteristics, only detailed enough to enable overall performance/cost estimation, and that a detailed design of an entire plant is far beyond the scope of this investigation. Nonetheless, our approach here is consistent with the level of details applied in many other previous works.^{21,41–45} Component costs were calculated by multiplying the design geometries by ceramic vendor estimates for the individual parts. LM construction costs were scaled from LS-CSP designs using conservative assumptions (e.g., LS-CSP costs that included some material costs along with labor were taken as labor only costs for LM-CSP).

Non-designed subsystems were systems that were not given new geometries for the LM-CSP plant model and instead were estimated using conservative material factors and literature values. Example subsystems included the heliostat field, auxiliary components (pumps, spare parts, controls, and instruments), and power cycle. The parasitic losses, including both the pumping power and the heliostat tracking power, were recomputed for the LM-CSP case due to the significant impact on net power cycle efficiency, which affords LM-CSP a significant and important advantage.

All costs were normalized to a relevant performance parameter with the receiver subsystem costs normalized to receiver peak thermal output ($\$/kW_{tr}$), TES costs normalized to the stored energy capacity ($\$/kWh_t$), HX costs normalized to their respective thermal power ($\$/W_t$), and power cycle costs normalized to their peak electric power output ($\$/kW_e$). Normalized costs allow for direct comparison with other CSP designs and best illustrate the significance of LM-CSP exclusive components such as secondary concentrators (SCs), inert gas containment, and a separate receiver HTF (e.g., Sn) and TES fluid, which necessitates additional HXs.

Parasitic loads were calculated for the pressure loss and flowrates through the three HXs and were added to the heliostat field parasitic loss published for the LS-CSP plant. Additional O&M costs due to inert gas containment were added to the published O&M costs for the LS-CSP plant, which was mostly a function of the heliostat field. The ultimate conclusion is that LM-CSP can potentially reduce LS-CSP costs by $\sim 20\%$ or more for a power cycle efficiency of 60%.

IV. RESULTS AND DISCUSSION

The reader is directed to the [supplementary material](#) for further details regarding the cost model inputs and methodology used.^{58–89} Table III compares the materials used currently in LS-CSP plants operating at 565 °C and the proposed changes to enable LM-CSP at 1400 °C.

In addition to different materials, the LM-CSP plant detailed here required internal cavity receivers, TES HXs to transfer heat between the receiver and storage fluids, and inert atmosphere containment. The component costs were grouped into four sub-systems and normalized with respect to plant net electric output using a nominal efficiency of 60% for the LM-CSP plant's power cycle and 41% for the LS-CSP plant's power cycle (Fig. 6).

This roughly 20% reduction in initial capital costs translated to an equivalent reduction in the LCOE since fuel costs are zero and lifetime maintenance costs are not expected to be significantly different from a LS-CSP plant. Nitrogen containment was a significant system addition to the LM-CSP plant but did not significantly affect maintenance costs even if all the nitrogen is replaced several times annually (see the Inert Atmosphere Containment section in the [supplementary material](#)). The ceramics used in this design were thermodynamically stable with respect to the LMs chosen at high temperatures, which is not the case for 316 SS and molten

TABLE III. Material comparison between LS and LM CSP.

Subsystem	LS-CSP	LM-CSP
Receiver	Nickel alloy	Graphite
Receiver heat transfer fluid	Solar Salt (NaNO ₃ -KNO ₃)	Sn
TES fluid	Solar salt	Al-Si
TES tanks	Stainless Steel	Calcium aluminate cement
Power cycle HX	Stainless Steel	SiC
TES HX	Not Applicable	Calcium aluminate cement

salt. LS-CSP relies on slow reaction kinetics to achieve 20+ year life, whereas the materials used in the LM-CSP design presented here could remain inert almost indefinitely. However, further experimentation on the fatigue of ceramic components is required to guarantee long plant life beyond 30 years. The most significant uncertainties centered on the receiver design and construction costs, SC optical efficiency, as well as the power cycle cost and efficiency. If the LM receiver cost becomes half of what was modeled here, through further optimization, then the LM plant would become 27% less expensive than the LS plant, and conversely, if the receiver cost was twice of what was modeled here, the LM plant only becomes 9% less expensive. Thus, the receiver costs are a significant source of uncertainty, and it is important to address this in future work. This analysis considered 0.95 for the SC efficiency which was the product of the quartz window transmittance (0.97) and SC mirror reflectivity (0.98). If further heliostat field/SC optimization shows that the SC efficiency is reduced to 0.9, the heliostat field would increase an additional 5% and total plant costs would increase 1.5%. Plant costs were largely sensitive to power cycle efficiency, and Fig. 7 shows how the cost savings from the LS-CSP plant vary with the power cycle efficiency for the nominal design point presented.

Finally, significant uncertainties exist in achieving the required concentration ratio necessary for a 1400 °C receiver operating temperature. Further studies are needed, but this initial set of assumptions shows that SCs have a relatively small cost compared to the system and even with higher cost materials, the total plant cost is significantly reduced by the higher power block efficiency.

V. CONCLUSION

From this initial nominal LM CSP design, it is clear that the refractory materials, nitrogen containment, internal receiver geometry, and secondary concentration necessary for 1400 °C LM operation are not likely to be cost prohibitive. It is still acknowledged that other,

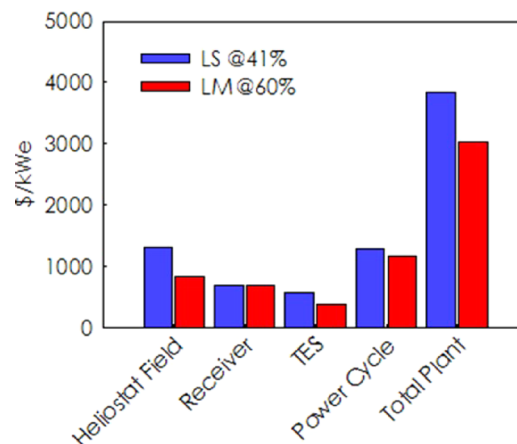


FIG. 6. Subsystem capital cost comparison.

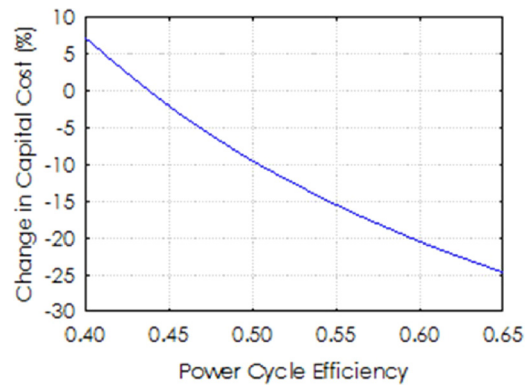


FIG. 7. LM-CSP plant reduction in capital costs vs. power cycle efficiency.

non-obvious costs that were not considered here could change this conclusion. Nonetheless, further study and investigation are strongly warranted, particularly since one of the major departures for LS-CSP, namely, the need for an inert containment system, could also be required for a high temperature molten chloride salt system (e.g., $Mg_2Cl-KCl$). While many of the materials and LM-CSP subsystems, such as the receiver, HXs, and pumps, were more expensive, the high temperature capability of LM potentially enabled a $\sim 50\%$ more efficient power cycle which could reduce LCOE by $\sim 20\%$ or more. Another key advantage of LMs was their high thermal conductivity, which ultimately led to greatly reduced parasitic losses compared to LS-CSP and further boosted the plant efficiency. The high energy density of two phase Al-Si decreased the size of LM containment tanks, leading to large reductions in TES subsystem costs despite requiring ceramics and inert atmosphere containment. The design and cost model presented here used conservative assumptions wherever possible, and it is likely that an optimized design could result in even greater cost reductions beyond $\sim 20\%$. Further experimental research is required to de-risk many of the components, particularly with respect to the secondary concentration, internal cavity receivers, and LDHX, but it is important to re-emphasize that the most critical risk, associated with the viability of the materials, seals and the ability to pump LM at these extreme temperatures has been reduced with recent LM experiments.³⁸ Thus, a continuous study of the LM-CSP concept seems to be warranted based on the estimates provided herein.

SUPPLEMENTARY MATERIAL

See [supplementary material](#) for the LM-CSP component designs and cost model.

ACKNOWLEDGMENTS

The authors are grateful for support from the U.S. Department of Energy, Advanced Research Projects Agency (ARPA-E) No. DE-AR0000339.

¹M. Mehos, C. Turchi, J. Jorgenson, P. Denholm, C. Ho, and K. Armijo, *On the Path to SunShot: Advancing Concentrating Solar Power Technology, Performance, and Dispatchability* (National Renewable Energy Laboratory (NREL), Golden, CO, USA, 2016).

²M. Woodhouse, R. Jones-Albertus, D. Feldman, R. Fu, K. Horowitz, D. Chung, D. Jordan, and S. Kurtz, *On the Path to SunShot: The Role of Advancements in Solar Photovoltaic Efficiency, Reliability, and Costs* (National Renewable Energy Laboratory (NREL), Golden, CO, USA, 2016).

³H. M. Branz, W. Regan, K. J. Gerst, J. B. Borak, and E. A. Santori, "Hybrid solar converters for maximum exergy and inexpensive dispatchable electricity," *Energy Environ. Sci.* **8**(11), 3083–3091 (2015).

⁴B. Dunn, H. Kamath, and J.-M. Tarascon, "Electrical energy storage for the grid: A battery of choices," *Science* **334**(6058), 928–935 (2011).

⁵H. Chen, T. N. Cong, W. Yang, C. Tan, Y. Li, and Y. Ding, "Progress in electrical energy storage system: A critical review," *Prog. Nat. Sci.* **19**(3), 291–312 (2009).

⁶G. J. Kolb, C. K. Ho, T. R. Mancini, and J. A. Gary, "Power tower technology roadmap and cost reduction plan," Report No. SAND2011-2419 (Sandia National Laboratories, Albuquerque, NM, 2011).

- ⁷M. Medrano, A. Gil, I. Martorell, X. Potau, and L. F. Cabeza, "State of the art on high-temperature thermal energy storage for power generation. Part 2—Case studies," *Renewable Sustainable Energy Rev.* **14**(1), 56–72 (2010).
- ⁸M. J. Wagner, S. A. Klein, and D. T. Reindl, "Simulation of utility-scale central receiver system power plants," paper presented at the ASME 2009 3rd International Conference on Energy Sustainability Collocated with the Heat Transfer and InterPACK09 Conferences, 2009.
- ⁹D. A. Baharoon, H. A. Rahman, W. Z. W. Omar, and S. O. Fadhil, "Historical development of concentrating solar power technologies to generate clean electricity efficiently—A review," *Renewable Sustainable Energy Rev.* **41**, 996–1027 (2015).
- ¹⁰M. Romero, R. Buck, and J. E. Pacheco, "An update on solar central receiver systems, projects, and technologies," *J. Sol. Energy Eng.* **124**(2), 98–108 (2002).
- ¹¹J. M. Lata, M. Rodríguez, and M. A. de Lara, "High flux central receivers of molten salts for the new generation of commercial stand-alone solar power plants," *J. Sol. Energy Eng.* **130**(2), 021002 (2008).
- ¹²G. J. Kolb, R. Davenport, D. Gorman, R. Lumia, R. Thomas, and M. Donnelly, "Heliostat cost reduction," paper presented at the ASME 2007 Energy Sustainability Conference, 2007.
- ¹³J. Leung, *Record-Breaking Cost Reductions for Solar Thermal Electricity Generation* (Estela Solar, 2017).
- ¹⁴C. Turchi, M. Mehos, C. K. Ho, and G. J. Kolb, "Current and future costs for parabolic trough and power tower systems in the US market," paper presented at the Proceedings of the 16th SolarPACES Conference, Perpignan, France, 2010.
- ¹⁵2020 Levelized Costs AEO 2015, *Independent Statistics & Analysis* (Energy Information Agency, 2017).
- ¹⁶M. T. Dunham and B. D. Iverson, "High-efficiency thermodynamic power cycles for concentrated solar power systems," *Renewable Sustainable Energy Rev.* **30**, 758–770 (2014).
- ¹⁷A. Kribus, R. Zaibel, D. Carey, A. Segal, and J. Karni, "A solar-driven combined cycle power plant," *Sol. Energy* **62**(2), 121–129 (1998).
- ¹⁸D. Kearney, B. Kelly, U. Herrmann, R. Cable, J. Pacheco, R. Mahoney, H. Price, D. Blake, P. Nava, and N. Potrovitza, "Engineering aspects of a molten salt heat transfer fluid in a trough solar field," *Energy* **29**(5), 861–870 (2004).
- ¹⁹A. G. Fernández, M. I. Lasanta, and F. J. Pérez, "Molten salt corrosion of stainless steels and low-Cr steel in CSP plants," *Oxid. Met.* **78**(5–6), 329–348 (2012).
- ²⁰A. Kruizenga and D. Gill, "Corrosion of iron stainless steels in molten nitrate salt," *Energy Procedia* **49**, 878–887 (2014).
- ²¹S. Goods and R. W. Bradshaw, "Corrosion of stainless steels and carbon steel by molten mixtures of commercial nitrate salts," *J. Mater. Eng. Perform.* **13**(1), 78–87 (2004).
- ²²B. Elkin, L. Finkelstein, T. Dyer, and J. Raade, "Molten oxide glass materials for thermal energy storage," *Energy Procedia* **49**, 772–779 (2014).
- ²³L. C. Olson, J. W. Ambrosek, K. Sridharan, M. H. Anderson, and T. R. Allen, "Materials corrosion in molten LiF–NaF–KF salt," *J. Fluorine Chem.* **130**(1), 67–73 (2009).
- ²⁴H.-S. Cho, J. W. V. Zee, S. Shimpalee, B. A. Tavakoli, J. W. Weidner, B. L. Garcia-Diaz, M. J. Martinez-Rodriguez, L. Olson, and J. Gray, "Dimensionless analysis for predicting Fe–Ni–Cr alloy corrosion in molten salt systems for concentrated solar power systems," *Corrosion* **72**(6), 742–760 (2016).
- ²⁵C. K. Ho and B. D. Iverson, "Review of high-temperature central receiver designs for concentrating solar power," *Renewable Sustainable Energy Rev.* **29**, 835–846 (2014).
- ²⁶C. Ho, J. Christian, D. Gill, A. Moya, S. Jeter, S. Abdel-Khalik, D. Sadowski, N. Siegel, H. Al-Ansary, L. Amsbeck, B. Gobereit, and R. Buck, "Technology advancements for next generation falling particle receivers," *Energy Procedia* **49**, 398–407 (2014).
- ²⁷J. Pacio, A. Fritsch, C. Singer, and R. Uhlig, "Liquid metals as efficient coolants for high-intensity point-focus receivers: Implications to the design and performance of next-generation CSP systems," *Energy Procedia* **49**, 647–655 (2014).
- ²⁸J. Pacio and T. Wetzel, "Assessment of liquid metal technology status and research paths for their use as efficient heat transfer fluids in solar central receiver systems," *Sol. Energy* **93**, 11–22 (2013).
- ²⁹Z. Ma, M. Mehos, G. Glatzmaier, and B. Sakadjian, "Development of a concentrating solar power system using fluidized-bed technology for thermal energy conversion and solid particles for thermal energy storage," *Energy Procedia* **69**, 1349–1359 (2015).
- ³⁰T. Tan and Y. Chen, "Review of study on solid particle solar receivers," *Renewable Sustainable Energy Rev.* **14**(1), 265–276 (2010).
- ³¹N. P. Siegel, C. K. Ho, S. S. Khalsa, and G. J. Kolb, "Development and evaluation of a prototype solid particle receiver: On-sun testing and model validation," *J. Sol. Energy Eng.* **132**(2), 021008 (2010).
- ³²Z. Ma and J. Martinez, "Fluidized-bed heat transfer modeling for the development of particle/supercritical-CO₂ heat exchanger," in *ASME 2017 11th International Conference on Energy Sustainability* (2017), p. V001T005A002.
- ³³V. Sobolev, "Database of thermophysical properties of liquid metal coolants for GEN-IV," SCK-CEN, Scientific Report No. BLG-1069 (2010).
- ³⁴Y. C. Yunshu Zhang, D. England, G. Wilk, F. DeAngelis, A. Henry, and K. Sandhage, "Containment materials for liquid metal based high temperature concentrated solar power: Compatibility with liquid tin," *J. Sol. Energy* **164**, 47–57 (2018).
- ³⁵E. Reed, "Stability of refractories in liquid metals," *J. Am. Ceram. Soc.* **37**(3), 146–152 (1954).
- ³⁶Y. Kurata and M. Futakawa, "Corrosion of CrN-coated steels in liquid Pb–Bi," *Mater. Trans.* **48**(3), 519–525 (2007).
- ³⁷Y. Zhao, C. Q. Cheng, Z. Y. Cao, and J. Zhao, "Interaction of liquid tin and zinc with AISI 304 stainless steel after passivation in air and nitric acid," *Mater. Charact.* **77**, 1–9 (2013).
- ³⁸C. Amy, D. Budenstein, M. Bagepalli, D. England, F. DeAngelis, G. Wilk, C. Jarrett, C. Kelsall, J. Hirschey, H. Wen, A. Chavan, B. Gilleland, C. Yuan, W. C. Chueh, K. H. Sandhage, Y. Kawajiri, and A. Henry, "Pumping liquid metal at high temperatures up to 1673 Kelvin," *Nature* **550**, 199 (2017).
- ³⁹A. DeAngelis, H. Seyf, R. Berman, G. Schmidt, D. Moore, and A. Henry, "Design of a high temperature (1350 °C) solar receiver based on a liquid metal heat transfer fluid: Sensitivity analysis," *J. Sol. Energy* **164**, 200–209 (2018).
- ⁴⁰P. Gilman and A. Dobos, *System Advisor Model, SAM 2011.12.2: General Description* (National Renewable Energy Laboratory (NREL), Golden, CO, 2012).
- ⁴¹C. S. Turchi and G. A. Heath, "Molten salt power tower cost model for the system advisor model (sam)," *Contract* **303**, 275–3000 (2013).

- ⁴²J. Wette, F. Sutter, A. Fernandez-Garcia, R. Lahlou, and P. Armstrong, *Standardizing Accelerated Aging Testing Conditions for Silvered-Glass Reflectors* (SolarPACES, 2017).
- ⁴³W. Kingery, "Thermal conductivity: XII, temperature dependence of conductivity for single-phase ceramics," *J. Am. Ceram. Soc.* **38**(7), 251–255 (1955).
- ⁴⁴N. S. Rasor and J. D. McClelland, "Thermal properties of graphite, molybdenum and tantalum to their destruction temperatures," *J. Phys. Chem. Solids* **15**(1), 17–26 (1960).
- ⁴⁵J. Murray and A. McAlister, "The Al-Si (aluminum-silicon) system," *Bull. Alloy Phase Diagrams* **5**(1), 74–84 (1984).
- ⁴⁶W. F. Gale and T. C. Totemeier, *Smithells Metals Reference Book* (Butterworth-Heinemann, 2003).
- ⁴⁷A. Goldsmith, *Handbook of Thermophysical Properties of Solid Materials: Elements* (Macmillan, 1961).
- ⁴⁸V. T. Cheang, R. A. Hedderwick, and C. McGregor, "Benchmarking supercritical carbon dioxide cycles against steam Rankine cycles for concentrated solar power," *Sol. Energy* **113**, 199–211 (2015).
- ⁴⁹V. Dostal, M. J. Driscoll, P. Hejzlar, and N. E. Todreas, "A supercritical CO₂ gas turbine power cycle for next-generation nuclear reactors," paper presented at the 10th International Conference on Nuclear Engineering, 2002.
- ⁵⁰S. A. Wright, R. F. Radel, M. E. Vernon, G. E. Rochau, and P. S. Pickard, "Operation and analysis of a supercritical CO₂ Brayton cycle," Sandia Report No. SAND2010-0171 (2010).
- ⁵¹A. Bruckner and A. Shariatmadar, "Heat transfer and flow studies of the liquid droplet heat exchanger," paper presented at the Space Nuclear Power Systems 1985, 1987.
- ⁵²M. Brewster, *Direct-Contact Heat Transfer* (Springer, 1988), pp. 167–195.
- ⁵³M. S. El-Genk and J.-M. Tournier, "Noble-gas binary mixtures for closed-Brayton-cycle space reactor power systems," *J. Propul. Power* **23**(4), 863–873 (2007).
- ⁵⁴G. Liu, M. Muolo, F. Valenza, and A. Passerone, "Survey on wetting of SiC by molten metals," *Ceram. Int.* **36**(4), 1177–1188 (2010).
- ⁵⁵W. L. Wang, Y. H. Wu, L. H. Li, W. Zhai, X. M. Zhang, and B. Wei, "Liquid-liquid phase separation of freely falling undercooled ternary Fe-Cu-Sn alloy," *Sci. Rep.* **5**, 16335 (2015).
- ⁵⁶K. McGowan, *Comparative Strengths of Refractories Versus Corundum in Furnace Linings* (Westmoreland Advanced Materials, 2008).
- ⁵⁷A. Henry and R. Prasher, "The prospect of high temperature solid state energy conversion to reduce the cost of concentrated solar power," *Energy Environ. Sci.* **7**, 1819–1828 (2014).
- ⁵⁸M. Mizuno, "Microstructure, microchemistry, and flexural strength of Mullite ceramics," *J. Am. Ceram. Soc.* **74**(12), 3017–3022 (1991).
- ⁵⁹W. T. Welford and R. Winston, *The Optics of Nonimaging Concentrators: Light and Solar Energy* (Academic Press, 1978).
- ⁶⁰R. Winston, J. C. Miñano, and P. G. Benitez, *Nonimaging Optics* (Academic Press, 2005).
- ⁶¹R. Pitz-Paal, N. B. Botero, and A. Steinfeld, "Heliostat field layout optimization for high-temperature solar thermochemical processing," *Sol. Energy* **85**(2), 334–343 (2011).
- ⁶²G. Wilk, *Liquid Metal Based High Temperature Concentrated Solar Power: Cost Considerations* (Smartech, 2016).
- ⁶³T. L. Bergman, F. P. Incropera, and A. S. Lavine, *Fundamentals of Heat and Mass Transfer* (John Wiley & Sons, 2011).
- ⁶⁴J. K. Dahl, K. J. Buechler, A. W. Weimer, A. Lewandowski, and C. Bingham, "Solar-thermal dissociation of methane in a fluid-wall aerosol flow reactor," *Int. J. Hydrogen Energy* **29**(7), 725–736 (2004).
- ⁶⁵A. Fernández-García, M. E. Cantos-Soto, M. Röger, C. Wieckert, C. Hutter, and L. Martínez-Arcos, "Durability of solar reactor materials for secondary concentrators used in CSP systems," *Sol. Energy Mater. Sol. Cells* **130**, 51–63 (2014).
- ⁶⁶G.-L. Dai, X.-L. Xia, and G.-F. Hou, "Transmission performances of solar windows exposed to concentrated sunlight," *Sol. Energy* **103**, 125–133 (2014).
- ⁶⁷B. D. Kelly, "Advanced thermal storage for central receivers with supercritical coolants," Report No. DOE/GO18149, 2010.
- ⁶⁸J. Stekli, L. Irwin, and R. Pitchumani, "Technical challenges and opportunities for concentrating solar power with thermal energy storage," *J. Therm. Sci. Eng. Appl.* **5**(2), 021011 (2013).
- ⁶⁹G. Glatzmaier, *Developing a Cost Model and Methodology to Estimate Capital Costs for Thermal Energy Storage* (National Renewable Energy Laboratory (NREL), Golden, CO, 2011).
- ⁷⁰N. Lorenzin and A. Abánades, "A review on the application of liquid metals as heat transfer fluid in concentrated solar power technologies," *Int. J. Hydrogen Energy* **41**(17), 6990–6995 (2016).
- ⁷¹S. S. A. N. Ghoiem, *Summary of Thermo-Physical Properties of Sn and Compounds of Sn-H, Sn-O, Sn-C, Sn-Li, and Sn-Si* (APEX Study, 2000).
- ⁷²M. S. Peters, K. D. Timmerhaus, R. E. West, K. Timmerhaus, and R. West, *Plant Design and Economics for Chemical Engineers* (McGraw-Hill, New York, 1968).
- ⁷³B. R. Munson, T. H. Okiishi, A. P. Rothmayer, and W. W. Huebsch, *Fundamentals of Fluid Mechanics* (John Wiley & Sons, 2014).
- ⁷⁴S. M. Ghiaasiaan, *Convective Heat and Mass Transfer* (Cambridge University Press, 2011).
- ⁷⁵R. Margolis, C. Coggeshall, and J. Zuboy, *SunShot Vision Study* (US Department of Energy, 2012), p. 2.
- ⁷⁶L. Vitos, A. Ruban, H. L. Skriver, and J. Kollar, "The surface energy of metals," *Surf. Sci.* **411**(1), 186–202 (1998).
- ⁷⁷C. T. Crowe, M. P. Sharma, and D. E. Stock, "The particle-source-in cell (PSI-CELL) model for gas-droplet flows," *J. Fluids Eng.* **99**(2), 325–332 (1977).
- ⁷⁸M. J. Moran, H. N. Shapiro, D. D. Boettner, and M. B. Bailey, *Fundamentals of Engineering Thermodynamics* (John Wiley & Sons, 2010).
- ⁷⁹J.-M. P. Tournier and M. S. El-Genk, "Properties of noble gases and binary mixtures for closed Brayton Cycle applications," *Energy Convers. Manage.* **49**(3), 469–492 (2008).
- ⁸⁰R. C. Wilcock, J. B. Young, and J. H. Horlock, "The effect of turbine blade cooling on the cycle efficiency of gas turbine power cycles," *J. Eng. Gas Turbines Power* **127**(1), 109–120 (2005).
- ⁸¹W. H. Stein and R. Buck, "Advanced power cycles for concentrated solar power," *Sol. Energy* **152**, 91–105 (2017).
- ⁸²T. M. L. Energetsko, "Energy-efficient gas-turbine blade-material technology—A review," *Energy* **355**, 361 (2017).
- ⁸³E. J. Burge, "A general review of closed-cycle gas turbines using fossil, nuclear and solar energy," *Phys. Bull.* **27**(8), 356 (1976).

- ⁸⁴M. Utamura, H. Hasuike, and T. Yamamoto, "Demonstration test plant of closed cycle gas turbine with supercritical CO," *Strojarsstvo* **52**(4), 459–465 (2010).
- ⁸⁵C. W. Forsberg, P. F. Peterson, and H. Zhao, "High-temperature liquid-fluoride-salt closed-Brayton-cycle solar power towers," *J. Sol. Energy Eng.* **129**(2), 141–146 (2006).
- ⁸⁶H. C. No, J. H. Kim, and H. M. Kim, "A review of helium gas turbine technology for high-temperature gas-cooled reactors," *Nucl. Eng. Technol.* **39**(1), 21–30 (2007).
- ⁸⁷H. Zhao and P. F. Peterson, "Multiple reheat helium Brayton cycles for sodium cooled fast reactors," *Nucl. Eng. Des.* **238**(7), 1535–1546 (2008).
- ⁸⁸L.-G. Chen, J.-L. Zheng, F.-R. Sun, and C. Wu, "Power, power density and efficiency optimization for a closed cycle helium turbine nuclear power plant," *Energy Convers. Manage.* **44**(15), 2393–2401 (2003).
- ⁸⁹X. Yan, K. Kunitomi, T. Nakata, and S. Shiozawa, "GTHTR300 design and development," *Nucl. Eng. Des.* **222**(2), 247–262 (2003).